ISSN 1674-1056
http://cpb.iphy.ac.cn
http://iopscience.iop.org/cpb
中国物理 B
Chinese Physics
中国物理
Chinese Physics B

Influence of N^+ implantation on structure, morphology, and corrosion behavior of Al in NaCl solution

Hadi Savaloni, Rezvan Karami, Helma Sadat Bahari, Fateme Abdi

Citation: Chin. Phys. B . 2020, 29(5): 058102 . **doi:** 10.1088/1674-1056/ab7d97
Journal homepage: http://cpb.iphy.ac.cn; http://iopscience.iop.org/cpb

What follows is a list of articles you may be interested in

Low-temperature plasma enhanced atomic layer deposition of large area HfS_2 nanocrystal thin films

Ailing Chang(常爱玲), Yichen Mao(毛亦琛), Zhiwei Huang(黄志伟), Haiyang Hong(洪海洋), Jianfang Xu(徐剑芳), Wei Huang(黄巍), Songyan Chen(陈松岩), Cheng Li(李成)

Chin. Phys. B . 2020, 29(3): 038102 . **doi:** 10.1088/1674-1056/ab6c4a

Influences of substrate temperature on microstructure and corrosion behavior of APS $Ni_{50}Ti_{25}Al_{25}$ inter-metallic coating

Sh Khandanjou, M Ghoranneviss, Sh Saviz, M Reza Afshar

Chin. Phys. B . 2018, 27(2): 028104 . **doi:** 10.1088/1674-1056/27/2/028104

Effects of annealing temperature on shape transformation and optical properties of germanium quantum dots

Alireza Samavati, Z. Othaman, S. K. Ghoshal, M. K. Mustafa

Chin. Phys. B . 2015, 24(2): 028103 . **doi:** 10.1088/1674-1056/24/2/028103

Aluminium phthalocyanine chloride thin films for temperature sensing

Muhammad Tariq Saeed Chani, Abdullah M. Asiri, Kh. S. Karimov, Atif Khan Niaz, Sher Bhadar Khan, Khalid. A. Alamry

Chin. Phys. B . 2013, 22(11): 118101 . **doi:** 10.1088/1674-1056/22/11/118101

Germanium nanoislands grown by radio frequency magnetron sputtering：Annealing time dependent surface morphology and photoluminescence

Alireza Samavati, Z. Othaman, S. K. Ghoshal, R. J. Amjad

Chin. Phys. B . 2013, 22(9): 098102 . **doi:** 10.1088/1674-1056/22/9/098102

Influence of N^+ implantation on structure, morphology, and corrosion behavior of Al in NaCl solution*

Hadi Savaloni†, Rezvan Karami, Helma Sadat Bahari, and Fateme Abdi

School of Physics, College of Science, University of Tehran, Tehran, Iran

(Received 9 December 2019; revised manuscript received 17 February 2020; accepted manuscript online 9 March 2020)

Structural and morphological changes as well as corrosion behavior of N^+ implanted Al in 0.6 M NaCl solution as function of N^+ fluence are investigated. The x-ray diffraction results confirmed AlN formation. The atomic force microscope (AFM) images showed larger grains on the surface of Al with increasing N^+ fluence. This can be due to the increased number of impacts of N^+ with Al atoms and energy conversion to heat, which increases the diffusion rate of the incident ions in the target. Hence, the number of the grain boundaries is reduced, resulting in corrosion resistance enhancement. Electrochemical impedance spectroscopy (EIS) and polarization results showed the increase of corrosion resistance of Al with increasing N^+ fluence. EIS data was used to simulate equivalent electric circuits (EC) for the samples. Strong dependence of the surface morphology on the EC elements was observed. The scanning electron microscope (SEM) analysis of the samples after corrosion test also showed that the surfaces of the implanted Al samples remain more intact relative to the untreated Al sample, consistent with the EIS and polarization results.

Keywords: aluminium, ion implantation, surface morphology, corrosion, electrochemical impedance spectroscopy, polarization

PACS: 81.65.Kn, 82.45.Bb, 52.77.Dq, 61.05.cp **DOI:** 10.1088/1674-1056/ab7d97

1. Introduction

Aluminium and its alloys are used in excess in different industries such as car, space, electronics, anodic materials for batteries, and cathode protecting systems, owing to their lightness, sheer strength, electrical and high thermal conductivity and corrosion resistance.[1–9] In spite of all these, because of their low hardness and low resistance, their use is limited.[2] In general, when the surface oxide layer of aluminium is dissolved, its surface becomes prone to corrosion which is due to the absorption of Cl^- ions that react with the Al cations in the oxide lattice.[9–11] This property of Cl^- ion is because of its small size and high penetration, strong anionic nature and the high dissolvability of chloride salt.[12,13] However, when metals and in particular Al are exposed to a polar environment/solvent (water or alcohol) or electrolyte solution (salt, acid, or alkali halides solved in water), the surface obtains an electrical potential because the water polar molecules have a negative extra charge on the oxygen atom and a positive charge on the hydrogen atoms, the electric forces from water molecules and metal atoms force the metallic ions to leave the material (metal) and move towards the solution as cations. This process is the mechanism of corrosion of a metal in the presence of an electrolyte such as sea water. Corrosion is defined as the interaction between a material (e.g., metal) and the corroding medium (environment) which leads to deterioration of the material and the environment.[14–16] Hence, the protection of the material from corrosion is of high importance. Use of different surface modification methods may provide ways to achieve this goal.[17–19]

Ion implantation modifies the sample surface and the interaction of the incident ions with sample atoms may lead to surface hardness and corrosion resistance of the sample surface.[20–26] In this process high temperatures are not required, while the bulk of the sample remains intact. Considering that in ion implantation one can control the ion fluence and the accelerating potential, hence conditions for tailoring the surface morphology are provided.[27]

It is shown that the corrosion resistance of the surface and its mechanical strength can be improved by N^+ ion implantation.[28–30] Ion implantation of Al surface leads to formation of an inhomogeneous hard AlN layer.[31–33] Researchers have shown that nucleation of AlN results in increasing of the surface hardness and decreasing of the erosion.[34] Also it is shown that both hardness and erosion of the Al surface depend on the fluence of the N^+ ions.[34] Abreu *et al.*[35] reported that implantation of nitrogen ions of 2×10^{17} ion/cm^2 with 50 keV energy leads to formation of AlN and improves the hardness, erosion, and corrosion resistance of AA7075 Al in NaCl medium.

N^+ ion implantation enhances the pitting type corrosion resistance considerably which in turn leads to the increase of the corrosion resistance of the sample. This can be due to the formation of a pinholeless AlN layer with no gaps between the grains.[21] In Ref. [36], the results of polarization measurements of N^+ ions implanted Al showed the enhancement of

*This work was funded by the University of Tehran.

†Corresponding author. E-mail: savaloni@khayam.ut.ac.ir

© 2020 Chinese Physical Society and IOP Publishing Ltd

corrosion resistance of the sample in seawater (0.6 M NaCl).

The Al surface hardness, corrosion, and wear resistance increase with N^+ ions implantation.[37–40] The influence of the substrate temperature and the condition of the N^+ ions beam on the modification of the surface by the nitride layer has been reported.[30,40–43]

Our aim in this work is to implant Al alloy (7049 with fifteen elements in its composition) substrate surface by N^+ ions of different fluences and study the corrosion behavior of these samples in 0.6 M NaCl solution (sea water simulated solution) using the electrochemical impedance spectroscopy (EIS) and polarization techniques. Correlation between the surface morphology/nanostructure and corrosion behavior of the samples (equivalent circuit elements) in corroding medium (NaCl solution) is also investigated.

2. Experimental details

Al samples (7049 with fifteen elements in its composition) (20 mm×20 mm×3 mm) were prepared for this study. Composition of Al was obtained by means of x-ray fluorescence (XRF) method (Philips PW2404, calibrate with Philips analytical x-ray B.V. standards with certificate of secondary for the SEMIQ). The results are given in Table 1. The Al samples were cleaned in heated acetone then ethanol using an ultrasonic bath. The cleaned Al samples were mounted on a holder in the implantation chamber.

Table 1. Chemical composition of Al (7049) used in this work.

Element	Zn	Mg	Cu	Cr	Si	Fe	S	Cl	K	Ca	Mn	P	Ga	Ti
Amount/wt.%	8.2	4.1	2.1	0.31	0.23	0.22	0.10	0.035	0.017	0.029	0.040	0.014	0.015	0.050

The N^+ ion implantation was performed under 2×10^{-5} mbar pressure at room temperature (298 K). The N^+ ions beam with different fluences of 1×10^{17} cm^{-2}, 3×10^{17} cm^{-2}, 5×10^{17} cm^{-2}, 7×10^{17} cm^{-2}, and 1×10^{18} cm^{-2}, N^+ ion energy of 30 keV, and ion current of 40 μA·cm^{-2} was used. Considering the definition of the current (number of ions per unit time) and having a fixed current, by increasing the ion fluence the required time for implantation increases (Table 2).

Table 2. Details of N^+ ions implantation process.

N^+ fluence/10^{17} cm^{-2}	1	3	5	7	10
Implantation time/s	360	1080	1800	2500	3600

The surface morphology and roughness of the samples were measured using an atomic force microscope (AFM: Nt-mdt scanning probe microscope, BL022, Russia; with low stress silicon nitride tip of less than 200 Å radius and tip opening of 18°). A STOE model STADI MP x-ray diffractometer, Germany (Cu K_α radiation) with a step size of 0.01° and count time of 1.0 s per step, was employed for crystallographic analysis of the samples. From the analysis of the two-dimensional (2D) AFM images, the average grain size and the surface roughness of the samples were obtained using JMicroVision and Nova Codes, respectively. The reproducibility of the results was confirmed by producing several samples (minimum of 4 samples for each implantation fluence) and checking the data at different stages of the work (different analyses; XRD, AFM, EIS, and polarization).

The electrochemical impedance spectroscopy (EIS) analysis of the samples was carried out using a potentiostat (Ivium, De Zaale 11, 5612 AJ Eindhoven, Netherlands) coupled to PC with reference to the open circuit potential (OCP) and in the frequency range of 100 kHz to 0.01 Hz with a voltage amplitude of 0.01 V. The sample (working electrode) was mounted in an inert fixture (polyamide) which only allows an area of 1 cm^2 of the sample surface being exposed to the 0.6 M NaCl solution and provids access to the back of the substrate for connection of an electrical contact, so that the working electrode is not influenced by undesirable effects. As the reference and the auxiliary electrodes a saturated calomel electrode and a platinum electrode were employed, respectively.

Before EIS measurement, the sample was immersed in the NaCl solution and the open circuit potential measurement was performed until it was stabilized.

The facility of the inert fixture mentioned above for connecting a copper wire to the back of the substrate was used to apply the polarization potential to the working electrode, where a saturated calomel reference electrode (SCE) and a platinum counter electrode were used in a three-electrode setup. The potential was swept with a rate of 1 mV·s^{-1} to cover a range of about 2 V for each sample, starting from −1 V vs. OCP. All measurements were performed at 298 K. All of the potentials presented in this work are as a function of SCE.

The corrosion current density j_{corr} and the corrosion potential E_{corr} were calculated from the Tafel extrapolation of the polarization curves of semi-logarithmic plot using the method prescribed in Ref. [44]. In order to make an accurate Tafel extrapolation, we started our extrapolation at least 50–100 mV away from E_{corr}. The polarization curves of the samples also showed at least one linear (semi-logarithmic) scale consistent with the prescription.[45,46]

The surface physical morphology of the samples after the polarization tests was obtained by means of scanning electron microscope (SEM: LEO 440i, England) analysis.

3. Results and discussion

3.1. XRD analysis

The XRD patterns of the implanted samples with N^+ ions of different fluences are given in Fig. 1. The spectra obtained for these samples contain a number of diffraction peaks with distinct difference between their intensities that cause difficulty in proper observation of their presence in the spectra. Therefore, in order to obtain a clear view of these peaks, we were forced to divide each diffraction spectrum into a few sections as presented in Fig. 1.

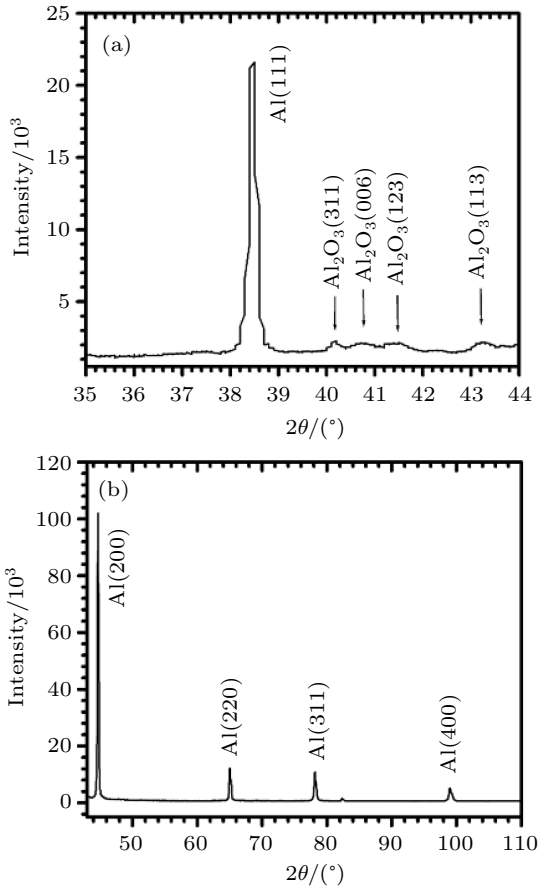


Fig. 1. XRD pattern of Al (alloy 7049 with fifteen elements).

In Fig. 1, the XRD pattern of the untreated Al sample shows nine peaks. Five of these peaks belong to the Al crystal phases of Al(111), Al(200), Al(311), Al(220), and Al(400) which appear at the following diffraction angles: $2\theta = 38.43°$, $2\theta = 44.69°$, $2\theta = 65.04°$, $2\theta = 78.15°$, $2\theta = 98.96°$, respectively, according to the JCPDS card No. 85-1327. The four remaining peaks at $2\theta = 40.12°$, $2\theta = 40.74°$, $2\theta = 41.50°$, and $2\theta = 43.29°$ can be related to Al_2O_3(311), Al_2O_3(006), Al_2O_3(123), and Al_2O_3(113) according to the JCPDS card Nos. 86-1410, 71-1684, 88-0107, and 42-1468, respectively. The XRD patterns of the implanted Al samples with different N^+ fluences in Fig. 2 show that the intensities of the Al peaks mentioned above are reduced compared to the untreated sample ones, while a secondary peak as a shoulder at a slightly higher diffraction angle is formed that after thorough investigation can be related to the aluminium nitride phases. The aluminium nitride peaks are formed at 44.80°, 65.20°, 78.39°, and 99.31° diffraction angles and belong to AlN(200), AlN(220), AlN(311), and AlN(400), respectively (according to the JCPDS card No. 46-1200). The results in this figure show that the intensity of the aluminium nitride peaks is increased with increasing N^+ ions fluence. In addition, the XRD patterns of the implanted samples show aluminum oxide phases Al_2O_3(002) and Al_2O_3(101) at 19.66° and 20.84° diffraction angles according to the JCPDS card Nos. 88-0107 and 73-1199, respectively. Also zinc nitride peaks are observed at 22.34°, 40.74°, and 41.50° diffraction angles that can be assigned to Zn_3N_2(211), Zn_3N_2(117), and Zn_3N_2(132), respectively (according to the JCPDS card Nos. 88-0618 and 30-1473).

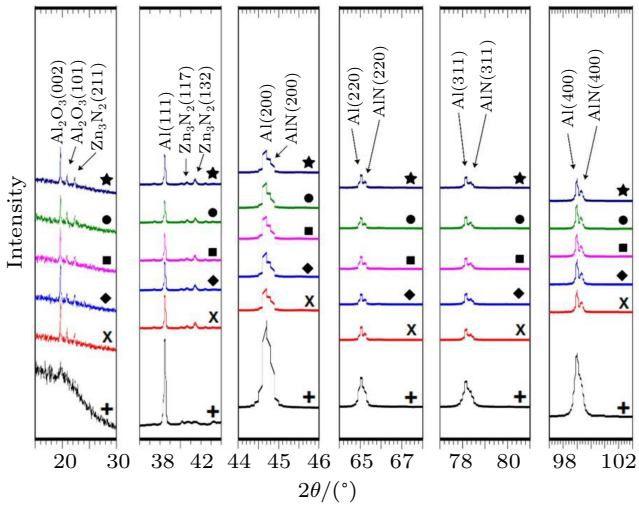


Fig. 2. XRD patterns for untreated Al (7049) and N^+ ion implanted Al (7049) samples with 30 keV energy and different fluences. +: untreated Al, ×: 1×10^{17} cm^{-2}, ♦: 3×10^{17} cm^{-2}, ■: 5×10^{17} cm^{-2}, •: 7×10^{17} cm^{-2}, ∗: 1×10^{18} cm^{-2}.

3.2. AFM analysis

The two- and three-dimensional AFM images of the untreated Al and N^+ ions implanted Al samples with different fluences are given in Figs. 3 and 4, respectively. The use of JMicroVision code on the 2D AFM images provides the information about the film surface roughness and grain size distribution in the produced samples (Table 3). Relatively large grains exist in the untreated Al sample (Fig. 3 and Table 3). However, when implanted with N^+ fluence of 1×10^{17} cm^{-2}, the grain size decreases and further increase of the N^+ ions fluence increases the grain size (Table 3). A number of processes may take place during the ion implantation; a) scattering from the grain boundaries, b) doping of the incident ions in the structure of the substrate (surface layers) and formation of smaller grains because of energetics of the incident ions which may break down the grain structure, c) transfer of energy of the ions to the substrate atoms and conversion of this

energy to heat which in turn enhances the diffusion effect and formation of larger grains. Therefore, one expects a competition between these processes and the final result will be due to domination of one or two of these processes. The initial decrease of the grain size could be due to grain boundary sputtering and breakdown of the grains due to penetration of the N^+ ions in the grain structure,[46] and the subsequent increase of the grain size could be due to the diffusion effect which enhances by increasing the N^+ ions fluence that in turn requires more time when a constant ion current is used for all fluences used in this work (Table 2). This process increases the amount of heat accumulated in the sample due to the energy conversion of the incident ions in the sample. Although the untreated Al sample contains large grains but the surface roughness of this sample is the highest among all samples (Table 3). The influence of these parameters on the corrosion behavior of the samples in this work will be quantified in the following sections where results of different analyses (e.g., EIS and polarization) are discussed. In this work, as mentioned above the grain size is increased with N^+ ions fluence, hence it may be suggested that the diffusion effect is the dominant process. The AFM images of the sample implanted with the lowest ions fluence (1×10^{17} cm^{-2}) show grains of 80–100 nm distributed on the surface with smaller grains with lower height in the areas between these grains. When the fluence of the N^+ ions is increased to 3×10^{17} cm^{-2}, 5×10^{17} cm^{-2}, 7×10^{17} cm^{-2}, and 1×10^{18} cm^{-2} (Fig. 4), the size of the grains increases and the number of grain boundaries decreases which in turn decrease the number of defects in the structure of the produced samples. The average surface roughness (R_{ave}) of all samples obtained from the AFM analysis is shown in Table 3. It can be observed that the surface roughness decreases with increasing fluence of the N^+ ions, which is again due to formation of larger grains and activation of the diffusion process. Both of these observations suggest enhanced corrosion resistance by increasing the N^+ ions fluence, which will be discussed by the data obtained from EIS and polarization measurements.

Table 3. Average grain sizes and surface roughness obtained from AFM images for untreated Al and N^+ ions implanted Al samples.

N^+ fluence/10^{17} cm^{-2}	Al	1	3	5	7	10
D/nm	248	175	198	263	292	307
R_{ave}/nm	59.0	11.2	10.7	9.9	8.4	6.1

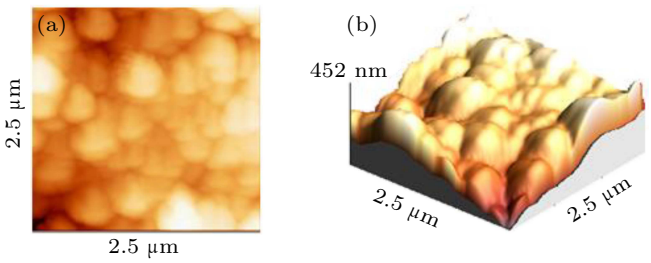


Fig. 3. The (a) 2D and (b) 3D AFM images of untreated Al (7049 alloy).

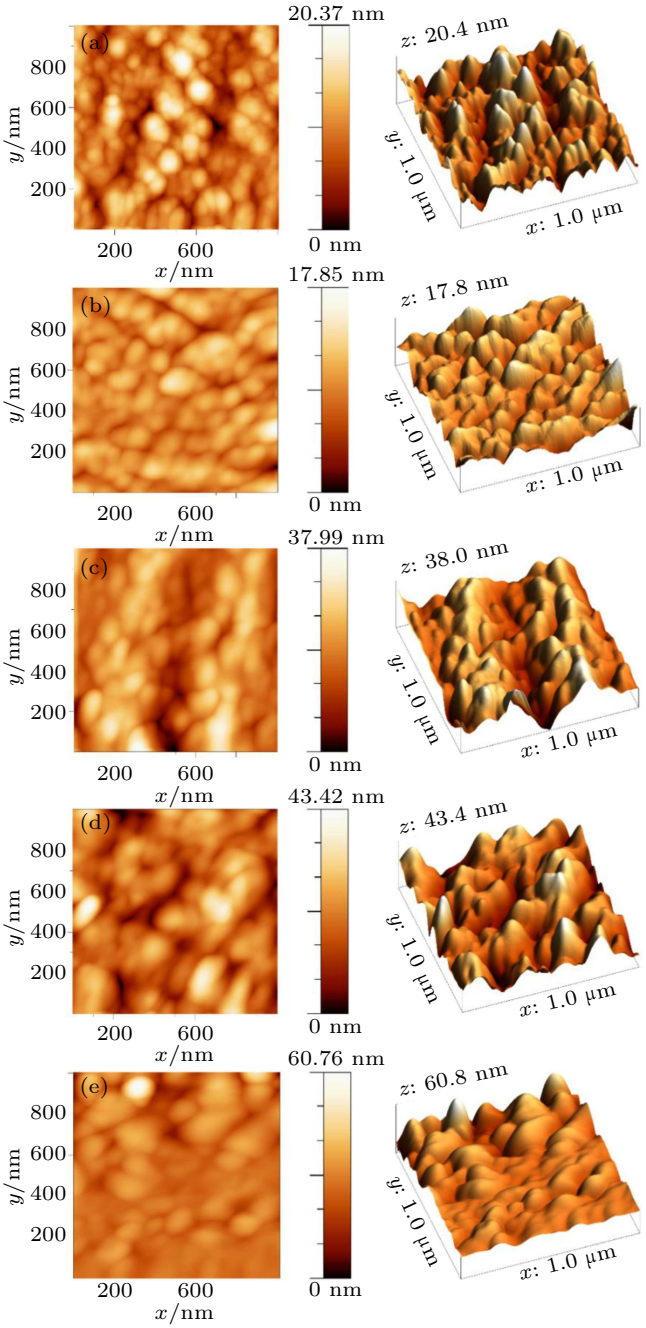


Fig. 4. The (a) 2D and (b) 3D images of N^+ ions implanted samples with different fluences; (a) 1×10^{17} cm^{-2}, (b) 3×10^{17} cm^{-2}, (c) 5×10^{17} cm^{-2}, (d) 7×10^{17} cm^{-2}, (e) 1×10^{18} cm^{-2}.

3.3. Electrochemical impedance spectroscopy

EIS is a nondistructive test, hence it was carried out on the sample before polarization measurement. The results of EIS (Nyquist plots) analysis of the untreated Al sample and Al samples implanted with N^+ ions of different fluences are given in Fig. 5. It can be observed that the corrosion resistance of the Al samples increases with N^+ ion fluence. The Nyquist plots of all samples with the exception of the highest (1×10^{18} cm^{-2}) N^+ ion fluence usually are treated as two semi-circles (time constants), while the highest N^+ fluence shows three semi-circles (time constants) (also discussed below using phase diagrams). The first semi-circle which occurs

at higher frequencies is indicative of the capacitance behavior of the sample (as a result of a positive phase difference of 90° between current and voltage). The second semi-circle also suggests the existence of another capacitor. The presence of this second capacitor may indicate the formation of an extra maximum in the phase diagram introduced in the following paragraphs.

These second capacitors are indicative of the capacitance (constant phase element) behavior of the interface between the undisturbed surface layer of Al by N^+ ions implantation (hereafter it is called "substrate") and the corroding medium (double layer) through incompleteness (pores/pinholes) of the modified/coated surface layer of Al by N^+ ions implantation (hereafter it is called "coating"). The value of this double layer capacitor depends on several factors such as the potential of the electrode, temperature, ionic density of the electrolyte solution, type of ions, and surface adsorption of impurities. The incompleteness of the coating allows the corroding medium to penetrate into the structure.

As mentioned above, the Bode and the phase diagrams which can be obtained through the best fit procedure between experimental data and the equivalent circuit (EC) provide more information that will be discussed further in the following paragraphs.

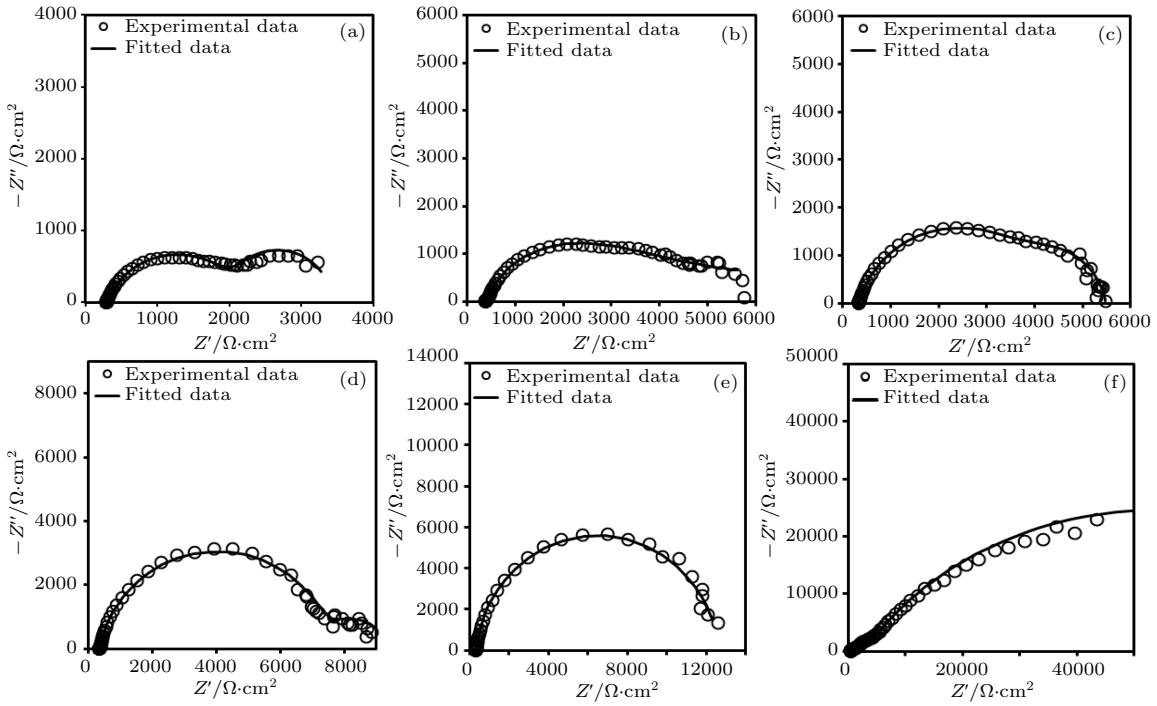


Fig. 5. Nyquist diagrams of (a) untreated Al alloy (7049) and N^+ ions implanted Al alloy (7049) with different fluences: (b) 1×10^{17} cm^{-2}, (c) 3×10^{17} cm^{-2}, (d) 5×10^{17} cm^{-2}, (e) 7×10^{17} cm^{-2}, (f) 1×10^{18} cm^{-2}.

In Figs. 6(a) and 6(b), the ECs for the untreated Al sample and the N^+ ions implanted samples produced in this work and discussed above are given. In these circuits, R_S is the solution resistance, CPE_1 is the capacitance (constant phase element) of the coating and given as

$$\mathrm{CPE}_1 = \varepsilon\frac{A}{d}, \tag{1}$$

where d is the thickness of the coating, A is the area of the sample exposed to the corroding medium, and ε is the dielectric constant of the coating. CPE_{dl} is the capacitance of the double layer. R_1 and R_{ct} are the pore and the charge transfer resistances related to CPE_1 and CPE_{dl}, respectively.

Due to the inhomogeneity of the structure of the formed layer and the roughness of the coated Al surface, CPE_1 and CPE_{dl} capacitors are not in an ideal state. Hence, n_1 and n_{dl} parameters may be assigned for the deviation of these capacitances from the ideal state (i.e., n for ideal state is unity). The EC to describe the highest N^+ ions fluence sample (Fig. 6(b)) is different from that of the rest samples, and R_2, CPE_2, and n_2 parameters are introduced. The phase diagram of this sample also shows three peaks (time constants). With regard to the addition of this third capacitor (constant phase element) and the change of EC in the case of the highest N^+ ions fluence, we may offer the following explanation. In case of ion implantation, one may use the theoretical (simulation) estimation of the distribution of N^+ ions of 30 keV energy used in this work for implantation in Al. This can be performed using simulation program TRIM2012 (transport of ions in matter), which is a group of programs that calculate the stopping power, average projected range ions (10 eV/amu to 2 GeV/amu), and other parameters involved in the implantation process using a quantum mechanical treatment of ion–atom collisions. The nominal N^+ ion average projected range (R_p = 69.9 nm),

straggling ($\Delta R_p = 26.7$ nm), maximum/peak N^+ concentration ($C_p = 1.4 \times 105$ atoms/cm) at the end of the implantation process (i.e., after 99999 ions implanted), are obtained from TRIM2012 calculations. Considering that the binding energy of the surface atoms on Al is not available, the heat of sublimation is used instead in the TRIM2012 calculation, which should not predict the realistic values and should be considered as a rough estimate. In addition, the roles of the ion fluence, that is the parameter investigated in this work, the temperature, and some other parameters such as surface roughening, hence the change of the surface binding energy are not included in TRIM2012 computer simulation code. However, one may make an estimation of the change of the N^+ ion distribution by increasing the N^+ ion fluence from the shape of the N^+ ions distribution considering Fig. 7 which is obtained for the calculation mentioned above and the skewness of the distribution. If we consider that by increasing the N^+ ion fluence the number of implanted N^+ ions increases and the heat accumulates in the substrate, hence the diffusion rate should increase and the ions may penetrate deeper in the substrate which in turn should increase the concentration and the skewness (this is a logical assumption), then at the highest N^+ fluence (assumed as the critical fluence), the tail of the distribution should smear deeper into the substrate (i.e., increase of skewness). Then one may relate the third capacitance (CPE_2) to the tail of the N^+ ion distribution in the Al substrate.

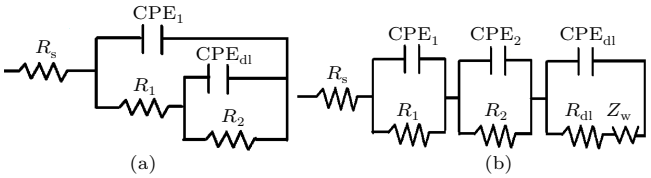


Fig. 6. Electrical equivalent circuits of (a) untreated Al alloy (7049) and N^+ ions implanted Al alloy (7049) samples with fluences of 1×10^{17} cm^{-2}, 3×10^{17} cm^{-2}, 5×10^{17} cm^{-2}, 7×10^{17} cm^{-2}, (b) N^+ ions implanted sample with fluence 1×10^{18} cm^{-2}.

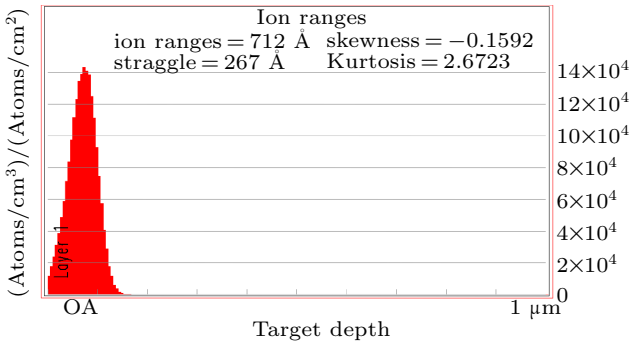


Fig. 7. Result of TRIM2012 code for N^+ ion distribution in Al sample after 9999 N^+ ion implantation.

The Bode and the phase diagrams for the samples discussed in this work resulted from the best fit procedure between the simulation and experimental data are compared in Fig. 8.

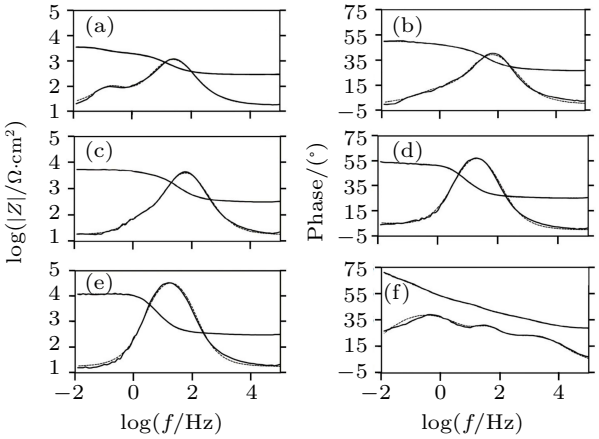


Fig. 8. Bode and phase diagrams for (a) untreated Al alloy (7049) and N^+ ions implanted Al alloy (7049) samples with different fluences: (b) 1×10^{17} cm^{-2}, (c) 3×10^{17} cm^{-2}, (d) 5×10^{17} cm^{-2}, (e) 7×10^{17} cm^{-2}, (f) 1×10^{18} cm^{-2}.

In Table 4, the quantities obtained from the fitting of EC in Fig. 5 to the experimental results are given. These values are obtained using the simulation procedure by the aid of Zsimp code. These results show that by implantation of 30 keV N^+ ions, the resistances (R_1, R_{ct} and in case of highest fluence R_2) are increased by increasing the N^+ ion fluence. Hence, the corrosion resistance of the Al sample improves with N^+ ion implantation in this work. This behavior is due to the formation of a nitride layer whose thickness/density increases with N^+ ions fluence relative to the native oxide layer on the surface of the Al sample before the implantation process. It can be observed that by increasing the N^+ ions fluence, the peak(s) of the phase diagram shifts to lower frequencies which is indicative of enhancement of corrosion behavior of the sample and the number of peaks in the phase diagram is representative of number of capacitors in the EC.

These are in agreement with the XRD results discussed in Subsection 3.1 (i.e., increase of aluminium nitride intensities with N^+ ion fluence). Therefore, it may be concluded that these variations in the characteristics of the samples are the cause for the increase of the corrosion resistance of the samples.

The decrease in CPE_1 and CPE_{dl} (and small value of CPE_2 in case of 1×10^{18} cm^{-2} N^+ fluence, while CPE_1 and CPE_{dl} of this sample are slightly increased relative to those of the other implanted samples) can be due to the increase of penetration (higher density) of the N^+ ions and the result of heat accumulation in the sample by increasing the implantation time (discussed above and in Subsection 3.2 (AFM results)). This leads to the formation of larger grains and a lower number of grain boundaries which in turn are responsible for the improvement of the corrosion resistance of the sample.

Table 4. Electrochemical parameters of untreated Al and implanted Al with N^+ ions of different fluences subjected to corrosion test in 3.5 wt% (0.6 M) NaCl solution, obtained from the simulation procedure using the Zsimp program.

	Al	1×10^{17} cm^{-2}	3×10^{17} cm^{-2}	5×10^{17} cm^{-2}	7×10^{17} cm^{-2}	1×10^{18} cm^{-2}
$R_s/\Omega\cdot cm^2$	336	343	327	340	324	339
$R_1/\Omega\cdot cm^2$	1384	1632	1739	6955	11970	17540
$CPE_1/\Omega^{-1}\cdot cm^{-2}\cdot s^n$	2.99×10^{-5}	5.59×10^{-6}	5.03×10^{-6}	4.84×10^{-6}	4.79×10^{-6}	6.94×10^{-5}
n_1	0.77	0.82	0.86	0.87	0.91	0.90
$R_2/\Omega\cdot cm^2$	–	–	–	–	–	43650
$CPE_2/\Omega^{-1}\cdot cm^{-2}\cdot s^n$	–	–	–	–	–	2.72×10^{-4}
n_2	–	–	–	–	–	0.90
$R_{ct}/\Omega\cdot cm^2$	1407	3438	3680	4774	5210	37480
$CPE_{dl}/\Omega^{-1}\cdot cm^{-2}\cdot s^n$	8.81×10^{-4}	3.07×10^{-4}	3.02×10^{-4}	2.17×10^{-4}	2.96×10^{-5}	4.47×10^{-5}
n_{dl}	0.69	0.47	0.51	0.61	0.60	0.61
$W/\Omega^{-1}\cdot cm^{-2}\cdot s^{0.5}$	–	–	–	–	–	9.97×10^{-7}
χ^2	0.0017120	0.0009673	0.0008349	0.0010770	0.0005905	0.0011350

3.4. Potentiodynamic determination

Polarization curves for untreated Al and N^+ ions implanted samples with different fluences are given in Fig. 9. The quantitative values of the electrochemical characteristics (i.e., corrosion potential and corrosion current density) resulted from fitting of Tafel slopes of the polarization curves are given in Table 5. In Fig. 9, it can be observed that (apart from the two samples produced with the highest N^+ ion fluences) with increasing the N^+ ions fluence, the corrosion potential is increased and the corrosion current is decreased, which indicate the improvement of the corrosion resistance of the implanted Al samples. This behavior can be attributed to the formation of Al nitride layer in the implanted samples. In another word, as mentioned before, by increasing the N^+ ions fluence, the grain size increases, the number of grain boundaries decreases, and the surface roughness of the samples decreases (see Subsection 3.2; AFM results), hence all of these changes occur in favor of enhancement of the corrosion behavior of the samples. The inferior behavior of the untreated Al sample although containing large grains could be due to the high surface roughness of this sample and deep valleys between the grains (due to defects) while the surface is not nitrided either. More careful investigation of the polarization curves in Fig. 9 shows that for the Al sample and the N^+ ion implanted samples with the lower three fluences, there is a clear passive potential ranging between −0.5 V and 0.1 V and at about 0.1 V, the pitting corrosion effect behavior can be distinguished. The pitting corrosion is clearly observed in these samples by SEM analysis and reported in the next section (see the inset of SEM images in Figs. 10(b)–10(d)).

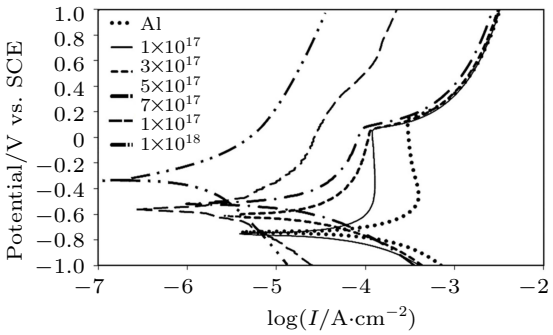


Fig. 9. Polarization curves of untreated Al alloy (7049) and N^+ ions implanted Al alloy (7049) samples with different fluences.

The polarization curves of the two samples produced with higher N^+ ion fluences do not show this pitting corrosion effect, and the corrosion current density is decreased to much lower values for these samples, especially for sample with the highest N^+ ion fluence of 1×10^{18} cm^{-2}. The results of polarization measurements are consistent with the EIS results and directly correlate with the structural and morphology of the samples discussed in different sections of this work.

Table 5. Corrosion potential and corrosion current densities for untreated Al and implanted Al with N^+ ions of different fluences subjected to corrosion test in 3.5 wt% NaCl solution, obtained from the polarization curves.

	Al	1×10^{17} cm^{-2}	3×10^{17} cm^{-2}	5×10^{17} cm^{-2}	7×10^{17} cm^{-2}	1×10^{18} cm^{-2}
E_{corr}/V (vs. SCE)	−0.73	−0.74	−0.62	−0.53	−0.55	−0.31
$i_{corr}/A\cdot cm^{-2}$	1.58×10^{-4}	6.07×10^{-5}	3.98×10^{-5}	2.51×10^{-5}	3.91×10^{-6}	1.67×10^{-6}

3.5. SEM analysis

In order to observe the physical changes of the surfaces of the samples after polarization test, the SEM images of the samples were taken and are shown in Figs. 10(a)–10(f). It can be seen that the sample implanted with the highest N^+ ions fluence (i.e., 1×10^{-8} cm^{-2}) remains almost intact (least damaged). The untreated sample after corrosion test clearly shows large cracks and pitting corrosion. When the Al sample has been subject to N^+ ion implantation with different fluences, these large cracks disappear even when the lowest N^+ ions fluence is used for implantation. The surface of the implanted samples shows the initial grooves/scratches which belong to

the initial surface of the as-received Al sample before implantation. As mentioned in the experimental section (Section 2), the Al alloy was used as received and no mechanical treatment (polishing and other techniques) was applied on them. Cleaning was only performed using ultrasonic bath with acetone and ethanol.

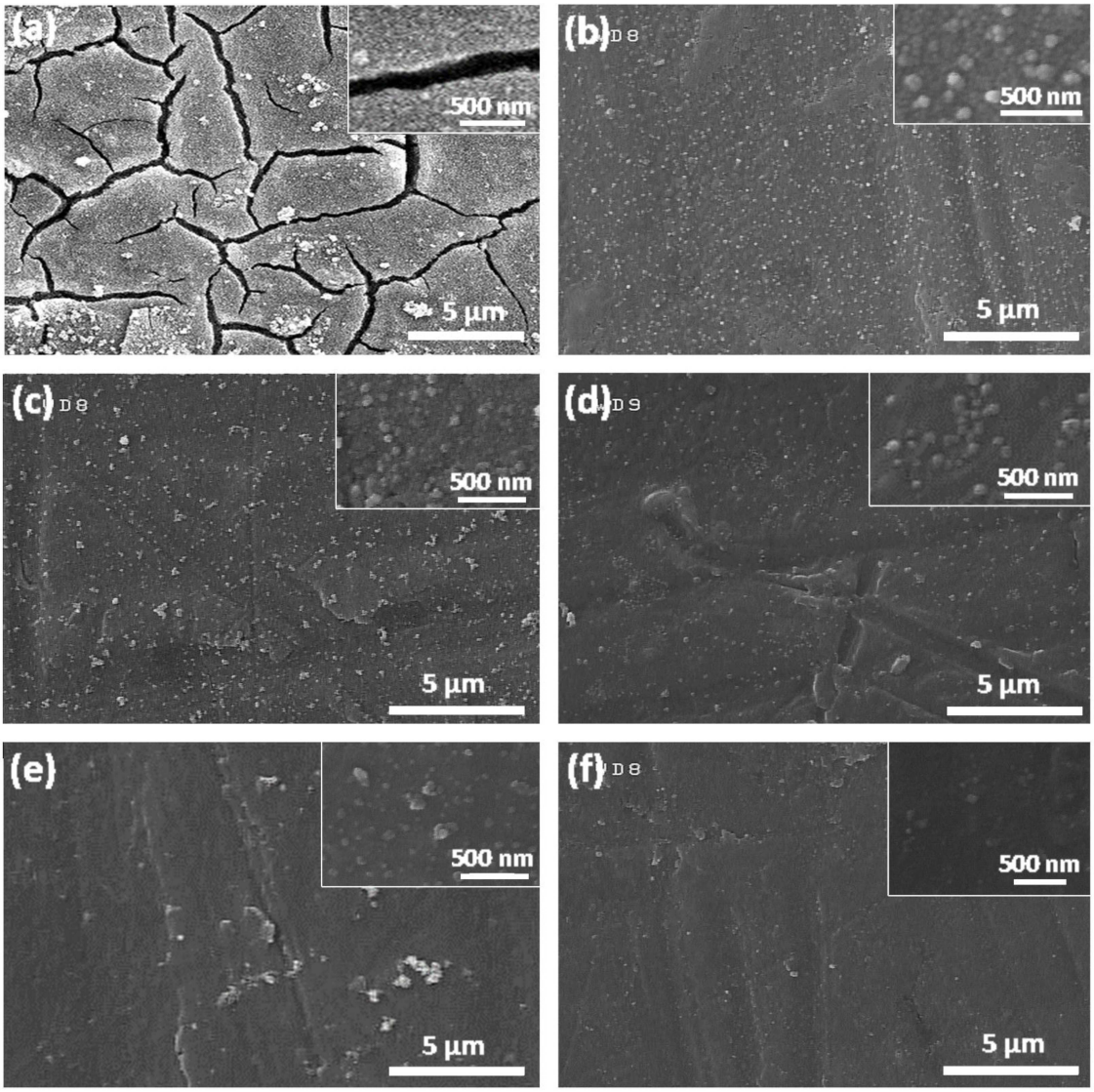


Fig. 10. FE-SEM images of untreated Al alloy (7049) and N^+ ions implanted Al alloy (7049) samples with different fluences after polarization tests: (a) untreated Al, (b) 1×10^{17} cm^{-2}, (c) 3×10^{17} cm^{-2}, (d) 5×10^{17} cm^{-2}, (e) 7×10^{17} cm^{-2}, (f) 1×10^{18} cm^{-2}.

4. Conclusions

Al type 7049 substrates were implanted with N^+ ions of different fluences. This process enhanced the corrosion resistance of the samples relative to the uncoated Al in 3.5% (0.6 M) NaCl solution. Both electrochemical impedance spectroscopy and polarization measurements showed that the highest corrosion behavior enhancement is achieved for the sample implanted with the highest N^+ ion fluence of 1×10^{18} cm^{-2}. Surface morphology and crystallographical structure of the samples were obtained using AFM and XRD, respectively, which showed the improvement of nitride phase and surface roughness, increase of grain size, and hence reduced number of grain boundaries with N^+ ions fluence. These results are in agreement and directly correlated with the electrochemical analyses.

Acknowledgement

This work was carried out with the support of the University of Tehran.

References

[1] Möller W, Parascandola S, Telbizova T, Günzel R and Richter E 2001 *Surf. Coat. Technol.* **136** 73
[2] Liu Y, Li L, Xu M, Cai X, Chen Q, Hu Y and Chu R K 2006 *Mater. Sci. Eng. A* **415** 140
[3] Sherif M E, Abdo H S, Khalil K A and Nabawy A M 2015 *Metals.* **5** 1799
[4] Bockris J O M and Kang Y 1997 *J. Solid. State. Electrochem.* **1** 17
[5] Sherif E M, Ammar H R and Khalil K A 2015 *Int. J. Electrochem. Sci.* **10** 775

[6] Fogagnolo J B, Velasco F, Robert M H and Torralba J M 2003 *Mater. Sci. Eng. A* **342** 131
[7] Sherif E M, Ammar H R and Khalil K A 2014 *Appl. Surf. Sci.* **301** 142
[8] Despić A R, Dražić D M, Purenović M M and Ciković N 1976 *J. Appl. Electrochem* **6** 527
[9] Sherif E M 2011 *Int. J. Electrochem. Sci.* **6** 1479
[10] Sherif E M 2013 *J. Ind. Eng. Chem.* **19** 1884
[11] Foley R T and Nguyen T H 1982 *J. Electrochem. Soc.* **129** 464
[12] Asaduzzaman M D, Mohammad C M and Mayeedul I 2011 *Chem. Ind Chem. Eng. Q* **17** 477
[13] Ibrahim M A M, Abd El Rehim S S and Hamza M M 2009 *Mater. Chem. Phys.* **115** 80
[14] Khandanjou S H, Ghoranevss M, Saviz S H and Afshar R 2018 *Chin. Phys. B* **27** 028104
[15] Feng X, Lei J, Gu H and Zhou S 2019 *Chin. Phys. B* **28** 026802
[16] Groysman A 2010 *Corrosion for everybody* (Germany: Springer)
[17] Meletis E I, Nie X, Wang F L and Jiang J C 2002 *Surf. Coat. Technol.* **150** 246
[18] Frignani A, Zucchi F, Trabanelli G and Grassi V 2006 *Corros. Sci.* **48** 2258
[19] Liu T, Zhang F, Xue C, Li L and Yin Y 2010 *Surf. Coat. Technol.* **205** 2335
[20] Dai L, Bi D, Hu Z, Liu X, Zhang M, Zhang Z and Zou S 2018 *Chin. Phys. B* **27** 048503
[21] Booske J H, Zhang L, Wang W, Mente K, Zjaba N, Baum C and Shohet J 1997 *J. Mater. Res.* **12** 1356
[22] Zhang L, Booske J H and Shohet J L 1995 *Mater. Lett.* **22** 29
[23] McCafferty E 2001 *Corros. Rev.* **57** 1011
[24] Gunzel R, Wieser E, Richter E and Steffen J 1994 *J. Vac. Sci. Technol. B.* **12** 927
[25] Walter K C 1994 *J. Vac. Sci. Technol. B* **12** 945
[26] Lucas S and Chevallier J 1994 *Surf. Coat. Technol.* **65** 128
[27] Fayeulle S 1998 *Defect. Diffus. Forum.* **57** 327
[28] Rondelli G, Vicentini B and Cigada A 1995 *Mater. Corros.* **46** 628
[29] Xia L, Wang R, Ma X and Sun Y 1994 *J. Vac. Sci. Technol. B.* **12** 931
[30] Lucas S, Chevallier J and Chechenin N G 1994 *Surf. Coat. Technol.* **66** 334
[31] Guzman L, Bonim G, Adami M, Ossi P M, Miotello A, Vittori-Antisari M, Serventi A M and Voltolini E 1996 *Surf. Coat. Technol.* **83** 284
[32] Jervis T R, Lu H L and Tesmer J R 1992 *Nucl. Instr. Methods B* **72** 59
[33] Lin C, Li Y, Kilner J A, Chater R J, Li J, Zhang J P and Hemment P L F 1993 *Nucl. Instr. Methods B* **80** 323
[34] Rodriguez R J, Sanz A, Medrano A and Garsia-Lorente J A 1999 *Vacuum* **52** 187
[35] Abreu C M, Cristobal M J, Figueroa R and Pena G 2015 *Appl. Surf. Sci.* **327** 51
[36] Walter K C, Dodd R A and Conrad J R 1995 *Nucl. Instrum. Methods. Phys. Res. B* **106** 522
[37] Manova D, Schreck M, Mändl S, Stritzker B and Rauschenbach B 2002 *Surf. Coat. Technol.* **151–152** 72
[38] Bilek M M, McKenzie D R, Tarrant R N, Oates T W, Ruch P, Newton-McGee K, Shi Y, Tompsett D, Nguyen H C, Gan B K and Kwok D 2004 *Contrib. Plasma. Phys.* **44** 465
[39] Saklakoglu I E 2009 *J. Mater. ProcessTechnol.* **209** 1796
[40] Richter E, Günzel R, Parasacandola S, Telbizova T, Kruse O and Moller W 2000 *Surf. Coat. Technol.* **128–129** 21
[41] Budzynski P, Youssef A A, Surowiec Z and Paluch R P 2007 *Vacuum* **81** 1154
[42] Piette M, Terwagne G, Moller W and Bodart F 1989 *Mater. Sci. Eng. B.* **2** 189
[43] Schoser S, Bräuchle G, Forget J, Kohlhof K, Weber T, Voigt J and Rauschenbach R 1998 *Surf. Coat. Technol.* **103–104** 222
[44] Stansbury E E and Buchanan R A 2000 *Fundamentals of Electrochemical Corrosion* (Ohio: ASM International)
[45] Poorqasemi E, Abootalebi O, Peikari M and Haqdar F 2009 *Corros. Sci.* **51** 1043
[46] Khojier K and Savaloni H 2009 *Vacuum* **84** 770